Forward Sweep—A Favorable Concept for a Laminar Flow Wing

G. Redeker* and G. Wichmann†
Deutsche Forschungsanstalt für Luft- und Raumfahrt e.V. (DLR), Braunschweig, Germany

The application of laminar flow on swept wings is authoritatively limited at high Reynolds numbers by a sweep angle where crossflow instability and attachment line transition lead to fully turbulent boundary layers on the wing. Theoretical and experimental investigations on finite swept wings show, because of three-dimensional displacement effects, an effective increase of wing sweep for backward swept wings and an effective decrease of wing sweep for forward swept wings compared to the geometrical sweep. For a laminar flow wing, the reduction in sweep in the case of a forward swept wing leads to a more stable laminar boundary layer concerning transition because of crossflow instability and attachment line transition. Thus, with this concept, a laminar forward swept wing can be realized more easily than a comparable swept back wing.

Nomenclature

c	= airfoil chord
c_l	= lift coefficient
c_p	= static pressure coefficient
d_r	= absolute wing thickness at wing root
d_t	= absolute wing thickness at wing tip
f	= frequency
M_∞	= freestream Mach number
N	= amplification exponent
Re	= Reynolds number based on wing chord
$\overline{Re}$	= characteristic Reynolds number for attachment line transition
s	= semispan
U_1	= slope of velocity normal to the wing leading edge
V	= velocity on wing contour
$V_{\min}$	= minimum of velocity (attachment line)
V_N	= component of velocity normal to wing leading edge
V_T	= component of velocity tangential to wing leading edge
V_∞	= freestream velocity
x_s	= surface coordinate in streamwise direction
x,y,z	= Cartesian coordinates
α	= angle of attack
β	= compressibility factor, $=\sqrt{1-M_\infty^2}$
$\Delta\varphi$	= additional sweep due to displacement effects
$\Delta\varphi_{\text{ink}}$	= additional sweep at $M_\infty = 0.1$
η	= dimensionless spanwise coordinate, $=z/s$
Λ	= wing aspect ratio
λ	= wing taper ratio
ν	= wing dihedral angle
φ	= geometrical wing sweep angle of leading edge
φ_{eff}	= effective sweep angle, $=\varphi+\Delta\varphi$
φ_{25}	= sweep angle of quarter chord line

Presented as Paper 88-4418 at the AIAA/AHS/ASEE Aircraft Design, Systems, and Operations Meeting, Atlanta, GA, Sept. 7–9, 1988; received March 27, 1989; revision received Feb. 21, 1990.

*Head, Section Airframe Aerodynamics, Institut für Entwurfsaerodynamik.
†Research Engineer, Institut für Entwurfsaerodynamik.

I. Introduction

THE application of laminar flow on swept wings is authoritatively limited at high Reynolds numbers by a certain sweep angle, where crossflow instability[1] and attachment line transition[2,3] lead to fully turbulent boundary layers on the wing. On the other hand, in order not to reduce the flight speed considerably as compared to today's transport aircraft, a certain sweep angle is required.[4] Thus, the design of a swept laminar flow wing is a compromise between contradicting demands.

When analyzing measured pressure distributions in the leading-edge region of a finite swept wing, it turned out that the pressure at the attachment line could not be reproduced by simple sweep theory with the sweep angle of the leading edge. As confirmed by experimental and theoretical investigations on finite swept wings, it will be shown that the geometrical sweep angle of a swept back wing is increased because of displacement effects of the fuselage and the wing itself. This leads to the definition of an effective sweep angle.[5]

Parametric studies of this effect, including the variation of aspect ratio, thickness ratio of wing tip/root, sweep angle, dihedral angle, and Mach number, will show the main influencing factors on the additional sweep angle $\Delta\varphi$.

It will be explained that for a forward swept wing this effect leads to a decrease in sweep compared to the geometrical sweep. Thus, for a laminar flow wing this reduction in sweep angle without influencing the flight speed results in a more stable laminar boundary layer with regard to crossflow instability and attachment line transition (see also Ref. 6). These effects will be discussed in some detail.

II. Effective Sweep

Considering the flow around complete aircraft configurations, three-dimensional displacement effects of wing, fuselage, and engine nacelle cause additional velocity components within the flowfield. Thus, the velocity of the flow along the wing leading edge is increased. Considering the sweep angle of the leading edge of finite wings, this effect leads to an effective sweep angle.[5]

First results from flight experiments[7] with the advanced technologies testing aircraft system (DLR-ATTAS) test airplane VFW-614 drew attention to this effect, leading to the definition of the effective sweep angle.

A. Definition of Effective Sweep Angle

In the summer of 1987, flight tests were performed with the DLR-ATTAS test airplane VFW-614 to investigate the stability of the laminar boundary layer of a swept wing.[8] The

evaluation of the test results requires a good knowledge of the leading-edge flow. Absolutely necessary is an accurate input of the leading-edge sweep angle for stability calculations,[9] because the stability of the laminar boundary layer around a swept wing leading edge is highly dependent on sweep angle.[10]

First evaluations of the flight tests showed that the real effective sweep angle had to be considerably higher than the corresponding geometrical sweep angle when analyzing the measured pressure distribution, especially in the wing leading-edge region.

Figure 1 shows an example of a measured pressure distribution of the midspan wing section of the VFW-614 ATTAS, as well as the corresponding velocity plot in the leading-edge region. Also indicated is the locus of the attachment line where the velocity reaches a minimum value. Decomposition of the velocity V normal and tangential to the leading-edge direction of the wing gives

$$V^2 = V_N^2 + V_T^2$$

At the locus of the attachment line, the velocity becomes a minimum:

$$V = V_T = V_{\min}$$

because $V_N = 0$.

Based on a simple sweep theory, a sweep angle φ_{eff} can be calculated as

$$\varphi_{\text{eff}} = \text{arc sin}(V_{\min}/V_\infty)$$

which turns out to be larger than the geometrical sweep angle of the leading edge.

Therefore, φ_{eff} is called the effective sweep angle and is defined as follows:

$$\varphi_{\text{eff}} = \varphi + \Delta\varphi$$

with φ as geometrical sweep of the considered configuration and an additional sweep angle $\Delta\varphi$, in which all contributions of the three-dimensional displacement effects are included.

For an infinite swept wing with sweep angle φ it follows that $\varphi_{\text{eff}} = \varphi$ and $\Delta\varphi = 0$ deg because there are no additional displacement effects in the spanwise direction.

For a finite wing with sweep angle φ, $\varphi_{\text{eff}} \neq \varphi$ and $\Delta\varphi \neq 0$ deg is obtained; i.e., additional displacement components have to be taken into consideration.

Thus, in the leading-edge region the problem of the finite wing with sweep angle φ is reduced to the case of an infinite swept wing with sweep angle φ_{eff}.

B. Theoretical and Experimental Investigations on a Finite Wing

In order to study effective sweep of a finite wing more deeply and to confirm the displacement effects found in the flight tests, theoretical investigations have been performed with the VFW-614 configuration. Analysis runs with a corresponding wing-body configuration, using the FLO30 code,[11] as well as with a wing alone using the FLO22 code,[12] have been carried out (Fig. 2).

The theoretical values of the effective sweep angle φ_{eff} have been determined from calculations of an average value for the velocity V_T along the leading edge in the nose region:

$$\varphi_{\text{eff}} = \text{arc sin}(V_T/V_\infty)_{\text{L.E.}}$$

The results are plotted in terms of

$$\Delta\varphi = \varphi_{\text{eff}} - \varphi$$

because this expression represents a direct measure of the additional three-dimensional displacement effects.

Since the boundary layers are very thin in the nose part of the wing, it seems justified to neglect viscous effects in the computations.

In Fig. 3, $\Delta\varphi$ for the VFW-614 configuration with and without body at Mach numbers 0.35 and 0.70 is presented. Plotted is the difference angle $\Delta\varphi$ vs the spanwise coordinate η. The displacement effects of wing and body cause an increase of sweep ($\Delta\varphi > 0$ deg), which is higher for the wing body (dashed line) than for the wing alone (full line). The contribution of the body is visible by the area between the curves and has its highest values near the wing root. In the tip region, the flow along the leading edge shows highly three-dimensional effects, resulting in high values of $\Delta\varphi$. The curves for the two Mach numbers show a similar behavior, but for the higher Mach number larger $\Delta\varphi$ values are calculated. Additional calculations varying angle of attack indicated no influence of α on $\Delta\varphi$ for the wing alone case, whereas for the wing-body case $\Delta\varphi$ increases with increasing incidence in the wing root region. The zigzag distribution of $\Delta\varphi$, as shown in this figure, is due to the rough leading edge of the original VFW-614 wing in spanwise direction.

In Fig. 4, a comparison of theoretical and flight tests results of the VFW-614 ATTAS is presented. The diagrams show values of $\Delta\varphi$ for the computed wing-body configuration, as well as the wing alone vs angle of attack, in comparison to results of the flight tests at a spanwise station of $\eta = 0.45$, which lie in the order of $\Delta\varphi \approx 2$–3 deg. The contributions of wing and fuselage to the total three-dimensional displacement can be separated very well from the theoretical results and are nearly independent of the angle of attack. The values of the corresponding flight measurements are clearly higher, because, on the real airplane configuration, an additional displacement effect may arise from the nacelle mounted upon the

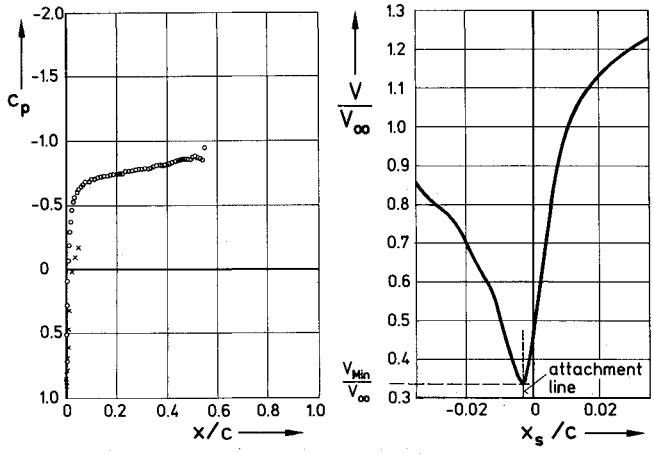

Fig. 1 Measured pressure and velocity distribution at wing midspan of the VFW-614 ATTAS airplane.

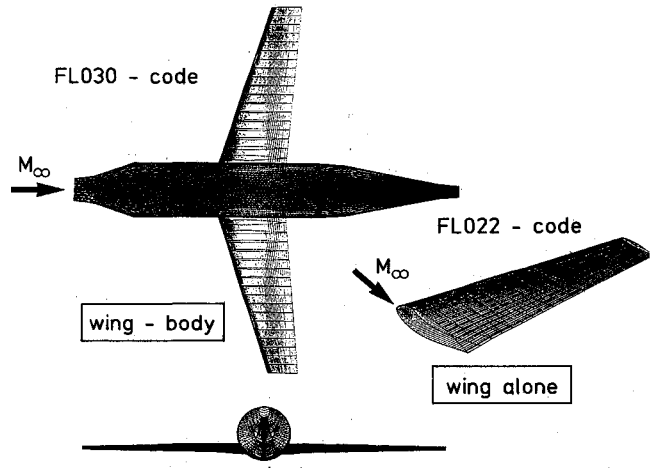

Fig. 2 Surface grids of the computed VFW-614 ATTAS configuration.

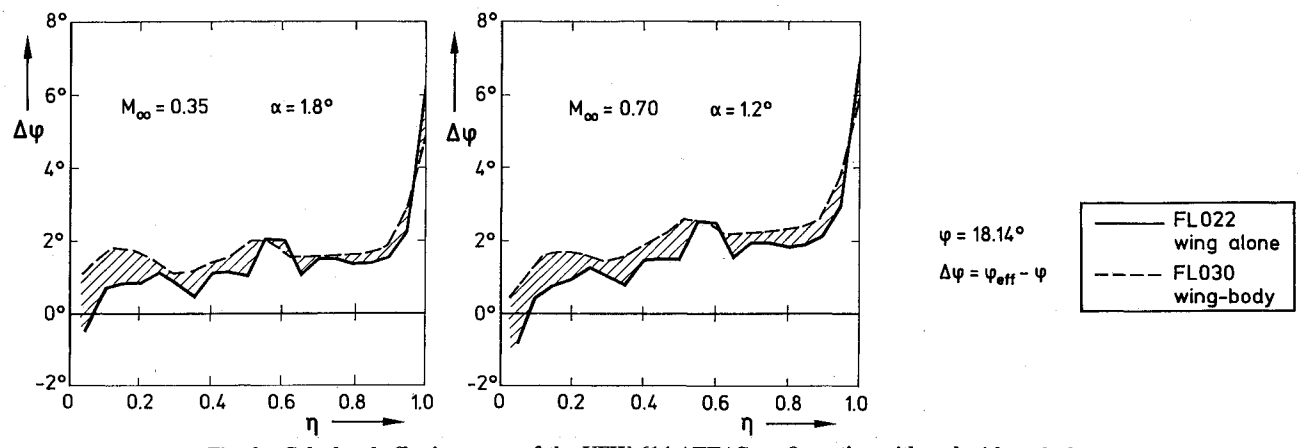

Fig. 3 Calculated effective sweep of the VFW-614 ATTAS configuration with and without body.

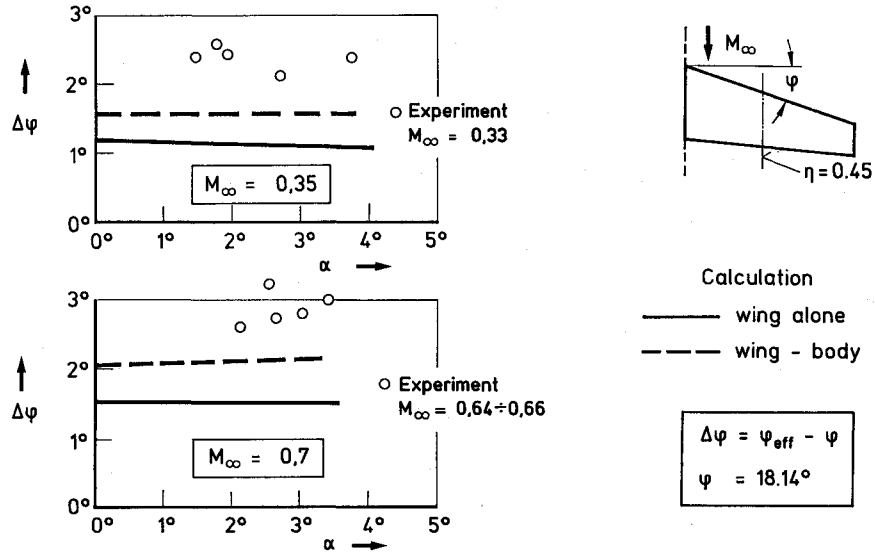

Fig. 4 Wing sweep increase $\Delta\varphi$ on a swept wing at midspan— comparison with flight test data.

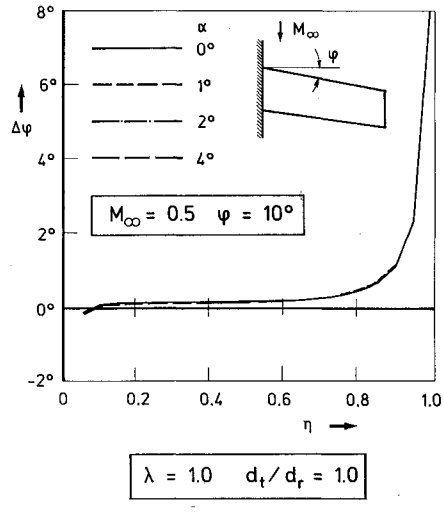

Fig. 5 Influence of angle of attack on the effective sweep angle.

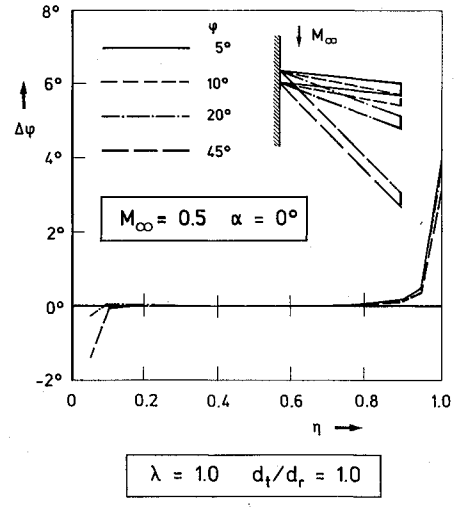

Fig. 6 Influence of geometrical wing sweep on the effective sweep angle.

upper wing surface. The scattering of measurement points can be explained by different flight conditions of the airplane. The results for the higher Mach number ($M_\infty = 0.7$) show higher values of $\Delta\varphi$ than for $M_\infty = 0.35$, indicating a Mach number influence.

In conclusion, the experimental as well as the theoretical results in the case of the VFW-614 ATTAS show that there is an increase of sweep near the leading edge that comes essentially from the three-dimensional displacement effects of the wing, body, and engine nacelles.

C. Parametric Studies

In order to separate the main influencing factors on the effective sweep angle, a detailed parametric study has been performed for a finite wing with a NACA 0012 wing section using the FLO22 code.

The following wing and flow parameters have been varied systematically: 1) angle of attack α, 2) geometrical leading edge sweep φ, 3) wing taper ratio λ, 4) wing aspect ratio Λ, 5) absolute wing thickness ratio (tip/root) d_t/d_r, 6) wing dihedral angle ν, 7) freestream Mach number M_∞.

The results are presented in the following figures. Figure 5 presents the influence of the angle of attack. The diagram $\Delta\varphi$ vs η shows that $\Delta\varphi$ is independent of wing incidence because no additional displacement is generated with varying α when the flow is symmetrical. The geometrical wing sweep angle φ has no influence on $\Delta\varphi$, as shown in Fig. 6. There are only slight differences at the wing root and tip for high sweep angles.

The influence of wing taper ratio on $\Delta\varphi$ is shown in Fig. 7. In order to separate the effect of taper ratio and thickness ratio, the absolute wing thickness ratio in spanwise direction was kept constant ($d_t/d_r = 1.0$). The calculations show that there is nearly no additional three-dimensional displacement effect due to wing taper and, thus, no influence on $\Delta\varphi$. The deviations of the curves to be seen in the figure are due to characteristic features of the analysis code.

Figure 8 presents the influence of the aspect ratio on $\Delta\varphi$. At high-aspect ratio ($\Lambda > 20$), $\Delta\varphi = 0$ deg, except the region near the wing tip. With decreasing Λ, $\Delta\varphi$ increases slightly and the midspan region is more and more influenced.

Figure 9 shows the influence of the absolute wing thickness ratio d_t/d_r on $\Delta\varphi$. The absolute wing thickness ratio is defined as the ratio of the absolute values of wing thicknesses at the tip and at the root. As can be seen in Fig. 9, there is a linear behavior between $\Delta\varphi$ and the absolute wing thickness ratio. With decreasing d_t/d_r, i.e., absolute wing thickness becoming smaller, $\Delta\varphi$ increases. As shown, this fact is valid for a rectangular wing as well as for a backward and forward swept wing. In contrast to the backward swept wing, $\Delta\varphi$ reduces the sweep angle φ of the forward swept wing.

The influence of the dihedral angle ν is presented in the case of a rectangular wing in Fig. 10. Depending on the sign of ν, either an increasing or decreasing $\Delta\varphi$ is obtained, being connected linearly with the angle of attack.

In order to establish the influence of the Mach number on $\Delta\varphi$, detailed investigations on a tapered wing with corresponding small values of the absolute wing thickness ($\lambda = 0.2$; $d_t/d_r = 0.2$) have been performed and are shown in Fig. 11. The upper part of the figure presents the distribution of $\Delta\varphi$ along the leading edge for $M_\infty = 0.1$, 0.3, 0.5, and 0.7. It can be stated that with increasing Mach number $\Delta\varphi$ also increases. The diagram plotted in the lower part of Fig. 11

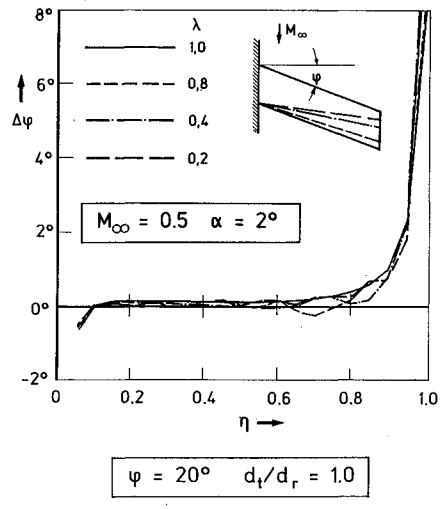

Fig. 7 Influence of wing taper ratio on the effective sweep angle.

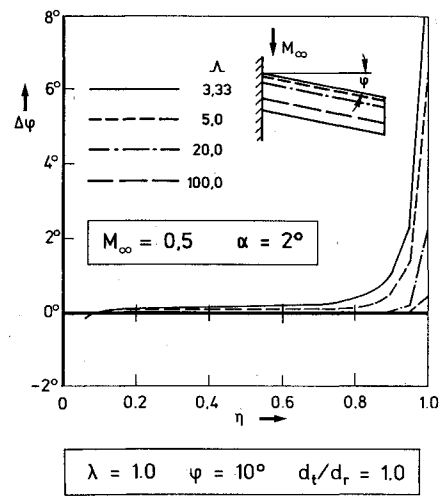

Fig. 8 Influence of wing aspect ratio on the effective sweep angle.

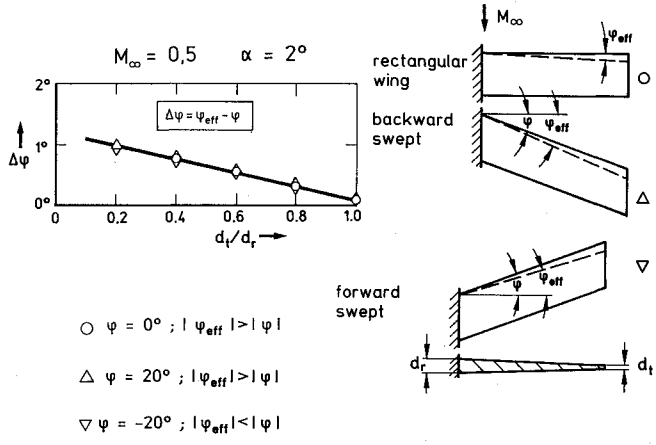

Fig. 9 Influence of absolute wing thickness ratio on the effective sweep angle.

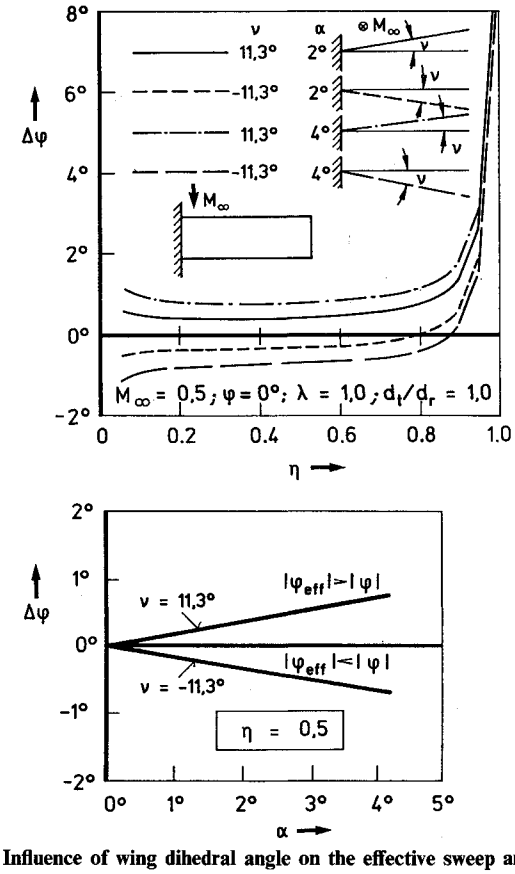

Fig. 10 Influence of wing dihedral angle on the effective sweep angle.

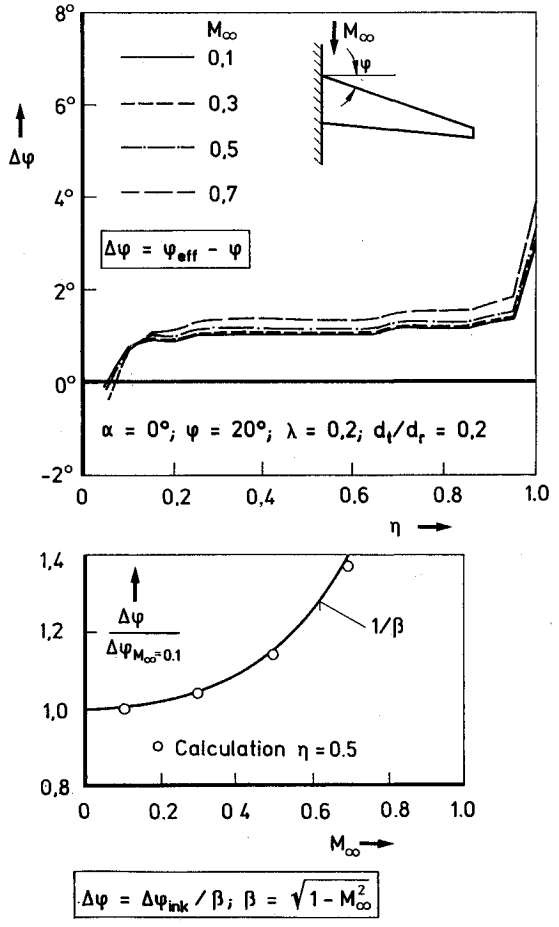

Fig. 11 Influence of Mach number on the effective sweep angle.

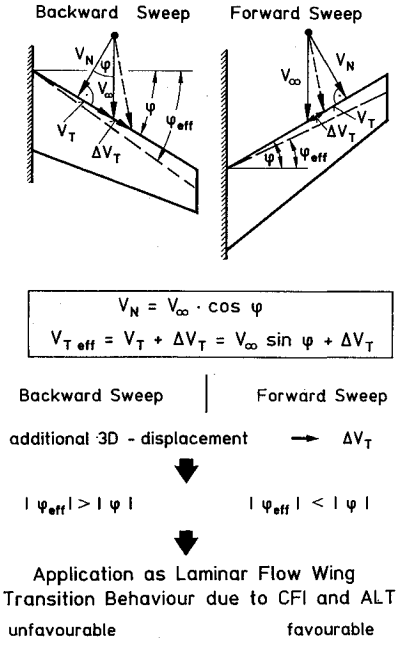

Fig. 12 Effective sweep of finite wings.

shows that the Mach number dependence follows the compressibility law after Prandtl and Glauert:

$$\Delta\varphi = \Delta\varphi_{\text{ink}}/\beta$$

with

$$\beta = \sqrt{1 - M_\infty^2}$$

From these figures it can be concluded that considerable large additional sweep angles $\Delta\varphi$ occur if wings with an absolute thickness ratio (tip/root) $d_t/d_r < 0.6$ are regarded. This case corresponds to the normal tapered wing of a transport aircraft. The effect is enlarged with increasing Mach number.

III. Influence of the Effective Sweep on the Design of a Laminar Flow Wing

In the preceding section it was pointed out that the additional sweep angle due to three-dimensional displacement effect has an increasing sweep effect in the case of a backward swept wing (BSW) and a decreasing sweep effect for a forward swept wing (FSW). This is summarized again in Fig. 12. Tapered backward and forward swept wings are compared with the same absolute value of the sweep angle φ of the leading edge. Due to three-dimensional displacement effects, an additional tangential velocity component ΔV_T occurs that, in the case of BSW, is added to the tangential velocity $V_T = V_\infty \cdot \sin\varphi$ at the leading edge. For the FSW case, ΔV_T has to be subtracted from V_T because of the opposite sign of V_T.

This leads the BSW to an effective sweep angle φ_{eff} that is larger than the geometrical sweep of the leading edge, whereas for FSW φ_{eff} is smaller than φ. This behavior results in some interesting features of such wings that are important for the application of the laminar flow technology.

On swept wings, transition from laminar to turbulent boundary layers can be described roughly by three transition mechanisms: the transition due to Tollmien-Schlichting instability (TSI),[13] to crossflow instability (CFI),[1] and to attachment line transition (ALT).[2,3]

The last two mechanisms are strongly dependent on the sweep angle of the leading edge of a swept wing. According to Pfenninger[2] and Poll,[3] the occurrence of attachment line transition will appear if a characteristic Reynolds number

$$\overline{Re} = \sin\varphi (Re/U_1)^{1/2}$$

exceeds a certain limiting value. Whereas $U_1 = d(V_N/V_\infty)/d(x_s/c)$ is the slope of the velocity normal to the leading edge at the attachment line, Re is the normal Reynolds number based on wing chord. This equation indicates that with increasing sweep angle φ, the danger of attachment line transition will also increase. If in the case of FSW the leading-edge sweep φ is decreased by a certain amount to the effective sweep angle φ_{eff}, a tapered FSW will have a favorable behavior compared to a tapered BSW, in view of attachment line transition.

In a recent paper, where a tapered BSW and FSW had been investigated with regard to attachment line transition, Poll and Paisley[6] stated: "It is suggested that a forward swept wing may be capable of supporting a laminar attachment-line flow at a much higher free-stream Reynolds number than a corresponding swept-back wing." This statement strongly supports our hypothesis of a smaller effective sweep angle in case of FSW.

The transition prediction due to crossflow instability of the laminar boundary layer can be made by a stability analysis[14] by means of the SALLY code.[15] In this procedure, transition takes place if the amplification exponent, or N factor, exceeds a certain value that has been determined from experiments.[16] The influence of the effective sweep angle on the N-factor development will be outlined in the following figures.

Figure 13 shows a typical pressure distribution of a basic airfoil of a natural laminar flow swept wing[10] that has been especially optimized for this purpose. The pressure distribution shown is that for the two-dimensional case for a wing section normal to the leading edge at $M_\infty = 0.74$, $Re = 20 \cdot 10^6$, and $c_l = 0.6$. This corresponds to a swept wing of $\varphi = 20$ deg sweep angle at $M_\infty = 0.79$ and $c_l = 0.53$.

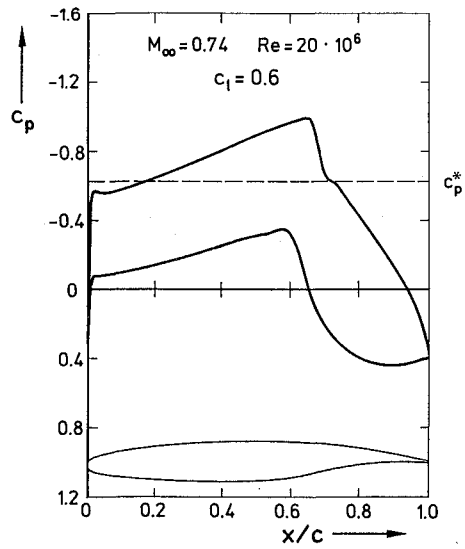

Fig. 13 Pressure distribution of the airfoil DLR-LV2 at $M_\infty = 0.74$ and $c_l = 0.6$.

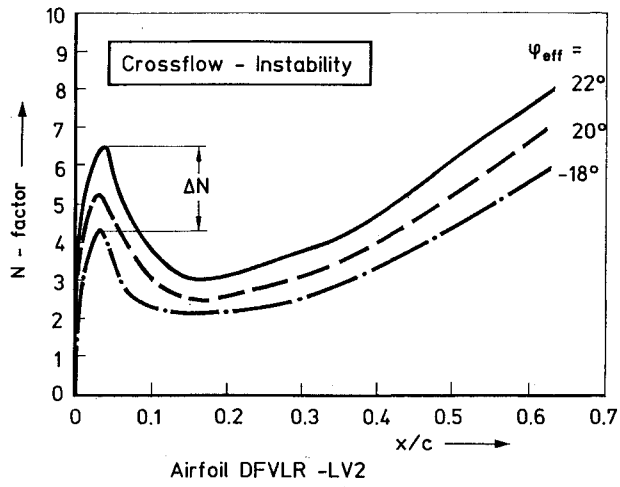

Fig. 14 Maximum of integrated N factor at $f = 0$ Hz for backward and forward swept wings.

If this pressure distribution is realized in a tapered forward and backward swept wing, an additional sweep angle of $\Delta\varphi \approx 2$ deg (according to Sec. II) can be estimated. This leads to $\varphi_{eff} = 22$ deg in the case of BSW and to $\varphi_{eff} = -18$ deg in case of FSW.

The result of a stability analysis of the crossflow mode at $f = 0$ Hz frequency (steady crossflow vortices) for three sweep angles $\varphi = 22$, 20, and -18 deg is shown in Fig. 14 as maximum integrated N factors along the wing chord. It is obvious that with increasing absolute value of sweep angle the maximum N value is increased, too. The difference between $\varphi = 22$ deg and $\varphi = -18$ deg is $\Delta N \approx 2.5$. From this figure it can be concluded that a forward swept wing due to smaller N values is more stable against crossflow instability than a backward wing with the same geometrical leading-edge sweep angle.

Furthermore, there are two aspects that make the FSW still more attractive. For a serious comparison of FSW and BSW, the leading-edge angle is not the adequate one. For a transport aircraft wing of large aspect ratio, the location of the local lift force is near to the quarter chord line of the wing; therefore, it seems justified to take this sweep angle φ_{25} as the comparison value. As demonstrated in Fig. 15, this procedure increases the leading edge sweep of BSW and decreases it on

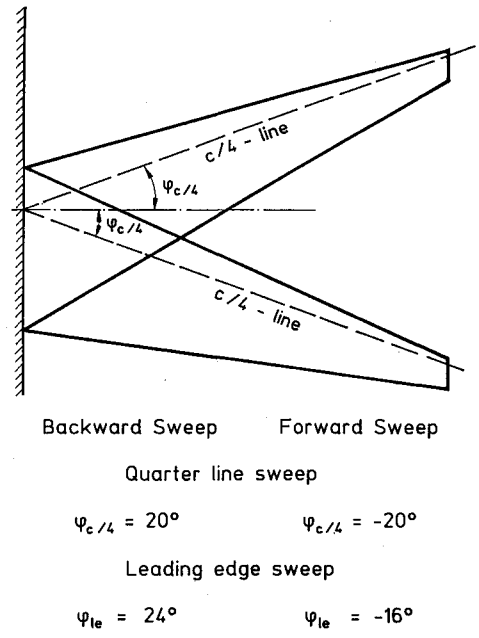

Fig. 15 Geometrical opposition of a backward and a forward swept wing with constant quarter line sweep.

the other hand of FSW. Thus, the difference in absolute value of sweep angle increases to 8 deg in this case. Together with $\Delta\varphi$, due to three-dimensional displacement effects, the forward swept wing will have a still smaller sweep angle than the backward swept wing.

The second point that should be mentioned here is that in case of BSW the turbulent boundary layer of the fuselage can spread along the leading edge, whereas in case of FSW no disturbances from the fuselage will contaminate the leading edge.

IV. Conclusions

Summarizing the results of the present paper, the following statements can be made:

1) On tapered backward swept wings, the geometrical sweep angle of the leading edge is increased by $\Delta\varphi$, due to three-dimensional displacement effects of the flow near the leading edge to an effective sweep angle. The value for $\Delta\varphi$ can be in the order of $\Delta\varphi \approx 2$ deg.

2) On tapered forward swept wings, the geometrical sweep angle of the leading edge is decreased by $\Delta\varphi$, due to three-dimensional displacement effects to an effective sweep angle, where $\Delta\varphi$ has the same order of magnitude as just mentioned.

3) These effects have been found on experiments with a backward swept wing and have been confirmed by calculations on backward and forward swept wings.

4) By means of a parametric study, it turns out that a small absolute wing thickness ratio (tip/root), which corresponds to normal wing taper, is the main influencing wing parameter generating additional sweep angles $\Delta\varphi$.

5) The existence of the effective sweep angle influences the application of a swept wing with regard to the laminar flow technology.

6) Forward swept wings are much more suited as laminar flow wings, due to a smaller effective sweep angle compared to a corresponding backward swept wing. Thus, the laminar boundary layer of a comparable forward swept wing is more stable against attachment line transition and crossflow instability.

References

[1]Owen, P. R., and Randall, D. J., "Boundary-Layer Transition on the Swept Back Wing," Royal Aircraft Establishment, TM-Aero 277, 1952.

[2]Pfenninger, W., "Laminar Flow Control. Laminarization," AGARD-R-654, 1977, pp. 3-1-3-75.

[3]Poll, D. I. A., "Transition in the Infinite Swept Attachment Line Boundary Layer," *The Aeronautical Quarterly*, Vol. 30, 1979, pp. 607–629.

[4]Redeker, G., "Aerodynamischer Entwurf von subsonischen Transportflugzeugen," DFVLR-IB, May 1980.

[5]Redeker, G., and Wichmann, G., "Untersuchungen zur effektiven Pfeilung am endlichen Tragflügel," 3. STAB Workshop, DLR, Göttingen, FRG, Nov. 1987.

[6]Poll, D. I. A., and Paisley, D. J., "On the Effect of Wing Taper and Sweep Direction on Leading Edge Transition," *Aeronautical Journal*, Vol. 89, 1985, pp. 109–117.

[7]Dressler, U., Horstmann, K.-H., and Redeker, G., "Erste Ergebnisser der Flugversuchsmessungen mit der VFW-614 ATTAS," 3. STAB Workshop, DLR, Göttingen, FRG, Nov. 1987.

[8]Horstmann, K.-H., Redeker, G., and Wichmann, G., "Auslegung des Laminarhandschuhs für die VFW-614 ATTAS," 3. STAB Workshop, DLR, Göttingen, FRG, Nov. 1987.

[9]Bieler, H., "Einfluß der numerischen Auflösung der Vorderkantenumströmung gepfeilter Flügel auf die lineare Störungsanfachung," 3. STAB Workshop, DLR, Göttingen, FRG, Nov. 1987.

[10]Redeker, G., Horstmann, K.-H., Köster, H., and Quast, A., "Investigations on High Reynolds Number Laminar Flow Airfoils," *Proceedings of 5th Congress of ICAS*, AIAA, New York, 1986, pp. 73–85.

[11]Shmilovich, A., and Caughey, D. A., "Application of the Multigrid Method to Calculations of Transonic Potential Flow about Wing-fuselage Combinations," Symposium on Multigrid Methods, NASA Ames Research Center, Moffett Field, Oct. 21–22, 1981.

[12]Jameson, A., and Caughey, D. A., "Numerical Calculation of the Transonic Flow Past a Swept Wing," Energy Research and Development Administration Report COO-3077-140, New York Univ., June 1977.

[13]Schlichting, H., *Boundary-Layer Theory*, 7th ed., McGraw-Hill, New York, 1979.

[14]Dagenhardt, J. R., "Amplified Crossflow Disturbances in the Laminar Boundary Layer on Swept Wings with Suction," NASA TP-1902, Nov. 1981.

[15]Srokowski, A. J., and Orszag, St. A., "SALLY Level II User's Guide," COSMIC PROGRAM LAR-12556, Athens, GA, 1979.

[16]Redeker, G., and Horstmann, K.-H., "Die Stabilitätsanalyse als Hilfsmittel beim Entwurf von Laminarprofilen," DGLR-Bericht 86-03, DGLR, Bonn, FRG, 1986, pp. 317–348.